# Plasmonic Gold Nanodiscs using Piezoelectric Substrate Birefringence for Liquid Sensing

Danni Hao, Mitchell G. Kenney, and David R. S. Cumming

*School of Engineering, Rankine Building, University of Glasgow, Glasgow, G12 8LT, UK*

This article presents the simulation, fabrication, and experimental characterization of a surface plasmonic resonance (SPR) sensor integrated with an acoustic sensing compatible substrate. The SPR sensor is designed to work in the visible region with gold nanodisc arrays fabricated on $LiNbO_3$, which is both piezoelectric and birefringent. A linear relationship between resonance wavelength and varying liquid refractive indices were observed in experiments, and a sensitivity of 165nm/RIU was obtained. Polarization effects of the birefringent property of the Y-cut $LiNbO_3$ substrate have been investigated, which can also be applied to X-cut $LiNbO_3$. Our study demonstrates the feasibility of an SPR sensor device utilizing a birefringent substrate, which has acoustic wave compatibility and can pave the way towards much more robust and flexible biosensing devices.

Both photonic and acoustic technologies are prominent in sensing applications where two important examples are surface plasmon resonance (SPR) sensors and surface acoustic wave (SAW) sensors, respectively. Traditionally, SPR sensors are made on non-piezo active glasses, hence for this investigation we have studied their behavior on a piezoelectric material. SPR can be exploited to create an enhanced electric field at the surface of metallic nanostructures (boundary between a metal and dielectric). At resonance, the field is strongly localized so that the exact characteristics of the associated spectrum are highly sensitive to the refractive index of any material that is close, or attached, to the surface. [1, 2] SPR biosensing can be achieved using metallic nanoparticles or from structured metallic thin films deposited on to a substrate - typically glass. Biosensors based on SPR possess many advantages such as high sensitivity, can be used in-situ, and possess label-free operation that are desirable for biosensing applications. [3, 4]

Surface acoustic wave sensors use interdigitated transducers (IDT) to generate and detect acoustic waves on the surface of the piezoelectric substrate, e.g. quartz, $LiNbO_3$ or $LiTaO_3$. A quantifiable change occurs in the resonance frequency and amplitude of the propagating wave that correlates to adsorbed mass, viscoelastic changes, and the conductivity of the surrounding liquid. [5] Unlike SPR, which is only sensitive to the bound molecule layer (in a liquid sample), acoustic sensors are not only sensitive to the binding molecules but also the viscosity of the solvent coupled to the biomolecule.[6] Whilst SPR can measure the mass of the adsorbed layer, an acoustic sensor can measure the viscous drag between the liquid and biomolecules, and determine the size and shape of the target biomolecule. [7] SAW devices can be used to induce a liquid flow by acoustic streaming, [8] and this phenomenon has been used in conjunction with a continuous metal film to accelerate and improve analyte capture for SPR sensing. [9, 10]

Such SPR sensors can be made by coating one surface of a prism with metal and measuring the change in the intensity of totally internally reflected light at different angles.[11] Studies have also been made with patterned metallic planar films in which surface modifications give rise to changes in the observed resonance characteristics.[2] The latter configuration reduces instrumentation complexity and can be rendered into a low-cost laboratory-on-a-chip (LOAC) format. [12, 13] The planar configuration of SAW devices is also suitable for LOAC formats. [9]

In this paper we investigate the potential for co-integration of acoustic and SPR technologies on a single device, and in particular to study the *optical* properties of SPR nanostructures on piezo-active materials. In order to do this we have selected the piezo-active material $LiNbO_3$, as it has high optical transmission (we obtain over 80% in visible range), large electromechanical coupling coefficients, as well as being optically birefringent unlike the glasses typically used to make SPR sensors. We present results on the refractive index dependent response of differing water-glycerine concentrations and polarization sensitivity of SPR nanostructures on $LiNbO_3$.

Crystalline $LiNbO_3$ can be cut on any of three planes to make X, Y or Z-cut surfaces, which are normal to crystallographic directions $[2\bar{1}\bar{1}0]$, $[1\bar{1}00]$, and $[0001]$, respectively.[14] In this study, we used samples from a 500 µm thick Y-cut wafer - a schematic diagram illustrating the crystallographic directions of $LiNbO_3$ is shown in Fig. 1(a). Due to the anisotropic nature of $LiNbO_3$ the refractive index for light normal to the Y-cut plane is sensitive to polarization. For an incident ray $k_o$ with the electric field in the direction of $[2\bar{1}\bar{1}0]$, then the refractive index is $n_o = 2.287$[15] whilst for an incident ray $k_e$ with electric field in the direction of $[0001]$, then $n_e = 2.203$[15].

Using the Y-cut $LiNbO_3$ as a substrate, arrays of gold nanodiscs were proposed as our SPR sensors in the configuration shown in Fig. 1(a). These were fabricated on the $LiNbO_3$ sample surfaces as follows: first, a 300 nm bi-layer PMMA was spin coated on to the $LiNbO_3$ surface; the resist was then prebaked on a hot-plate by ramping the temperature from 65 ˚C to 95 ˚C (since $LiNbO_3$ is a pyroelectric and can break when heated with a large temperature-gradient) for a total time of 8 minutes per coating; to avoid charging effects that can

damage $LiNbO_3$ when carrying out electron beam lithography (EBL), a 30 nm Al layer was evaporated on top of the resist, and EBL patterns were written at a beam voltage of 100 kV; following this, the protective Al layer was removed by MF-CD26 after the electron beam exposure; finally, after development in MIBK:IPA (1:2) solution, 60 nm Au was evaporated on to the sample with an initial 3nm Ti adhesion layer and the sample was then put into hot acetone for up to 4 hours for lift off. The final structure can be seen in Fig. 1(b), which was a square array of gold discs with a periodicity $a$ = 300 nm and a disc diameter $b$ = 180 nm (dimensions '$a$' and '$b$' are shown in the Inset of Fig. 1(b).)

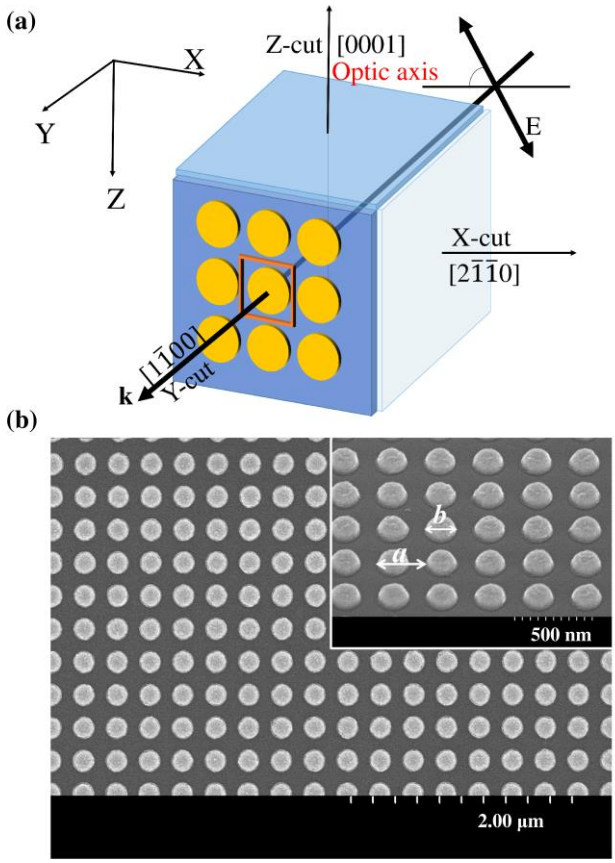


FIG. 1. (a) Schematic diagram showing gold nanodisc array and the crystal planes of the $LiNbO_3$. (b) A scanning electron micrograph of gold nanodiscs in a square array with a period of 300 nm on Y-cut $LiNbO_3$. Inset: a microscope image tilted at 45°, where $a$ and $b$ are the periodicity and disc diameter, respectively.

The transmission spectra of the gold nanodiscs on $LiNbO_3$ were simulated using *Lumerical FDTD*. A semi-infinite Y-cut $LiNbO_3$ substrate and a semi-infinite air/liquid superstrate were used to create the model. Two simulations with orthogonally polarized beams ($k_o$ and $k_e$) were performed. The net transmission for both polarizations (i.e. unpolarized light) was calculated using the arithmetic average of these simulations.[16] Periodic boundary conditions were defined along the $x$ and $z$ axes and perfectly matched layers were set at the top and bottom boundaries to absorb any unwanted reflections. A mesh cell with size of $\Delta x = \Delta y = \Delta z$ = 2 nm was set in the region encompassing the metal layer and part of the $LiNbO_3$ and air/liquid layer. In the simulations, Johnson and Christy's experimental values were used for the complex permittivity data of Au.[17]

Figure 2(a) shows the simulation result for applying water on top of the sensing surface for unpolarized light. Using an SPR sensor based on $LiNbO_3$, which has an approximate *average* refractive index of 2.25 (due to the anisotropy of $LiNbO_3$) for *unpolarized* light, and the water having a refractive index of 1.33, the large gap between these two refractive indices induces two resonance modes in the transmission spectra: a $LiNbO_3$ mode at $\lambda_B$ (where the subscript '$B$' means 'bottom'); and a liquid mode at $\lambda_T$ (where the subscript '$T$' means 'top'). The power distribution (inset Fig. 2(a)) shows that the resonance at $\lambda_T$ has a local maximum intensity at the top of the gold nanodisc – which is the interface of water and metal – whilst the resonance at $\lambda_B$ has a local maximum intensity at the bottom of the nanodisc – which is the interface of metal and $LiNbO_3$. Former SPR sensors based on glass appear to have only one resonance mode since the refractive index of the analyte is similar to that of glass ($n$=1.5) and the two modes hybridize together in the transmission spectra to give a broad response.[18]

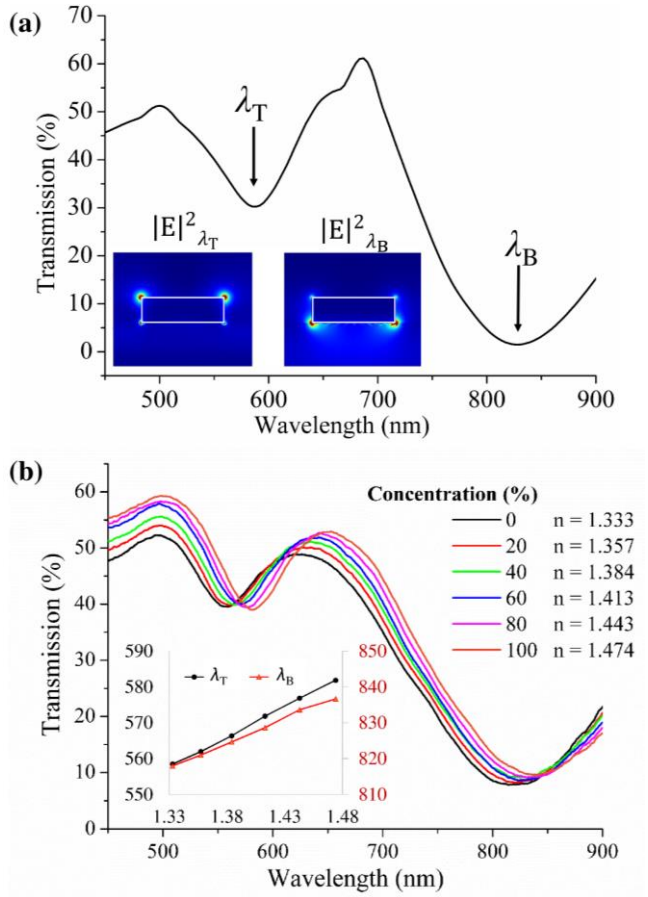


FIG. 2. (a) Simulated transmission spectrum for SPR sensors in water, where the two main resonance wavelengths are marked as $\lambda_T$ and $\lambda_B$. Inset: Electric field intensity distributions in the xy plane at $\lambda_T$ and $\lambda_B$, respectively. (b) Measured transmission spectra for the SPR sensors in a glycerin-water solution of differing concentrations. The average refractive index for each solution is given to the right of the concentration percentage. Inset: resonance wavelength (nm, y-axis) versus refractive index of glycerin-water solution (x-axis). The black curve is the resonance wavelength shift at liquid mode $\lambda_T$, and the red curve is the resonance wavelength shift at $LiNbO_3$ mode $\lambda_B$.

For biosensing applications, the variation of the resonance wavelength is mostly caused by the refractive index change in the analyte.[19] To confirm this, a series of glycerine-water solutions with different concentrations were applied on top of the surface of the SPR structures, where the refractive index of glycerine is 1.48 and differing concentrations of solution have refractive indices given by Ref. 20. The corresponding transmission spectra were measured using an Angstrom Sun Technologies Inc. microspectrophotometer MSP300, where an unpolarized light beam from a halogen lamp was normally incident on to the backside of the sample. Measured results are shown in Fig. 2(b). It was found that an increase in the glycerine-to-water concentration induces a redshift of the resonance wavelength modes for both $\lambda_T$ and $\lambda_B$. The resonance wavelengths were extracted and plotted as a function of the liquid refractive index in the inset of Fig. 2(b). A sensitivity of 165 nm per refractive index unit (RIU) has been observed at the liquid mode $\lambda_T$ and a sensitivity of 130 nm/RIU has been observed at the $LiNbO_3$ mode $\lambda_B$. The sensitivity for the liquid mode is comparable to other similar SPR sensors on isotropic media with a resonance in the same wavelength range[18] – for these, the sensitivity increases for longer resonant wavelengths,[21] but this principle only applies due to the similarity of substrate and superstrate refractive indices and yields only one broad resonance: for our structure it does not hold true for the higher wavelength $\lambda_B$ mode compared to $\lambda_T$. In essence, it can be inferred that it is the liquid (top) resonance mode $\lambda_T$ which provides the high sensitivity and undergoes a sensitivity increase for longer wavelengths.

Since $LiNbO_3$ has two distinct values for its refractive index (due to birefringence), it is necessary to evaluate the characteristics of the SPR structure with respect to the crystal orientation. We have therefore studied the behavior of the device in response to a changing polarization by varying the orientation of the E-field from 0° (aligned to the x-cut axis) to 90°, whilst normally incident to the xz plane. The transmission spectra in Fig. 3(a) shows how the resonance wavelength shifts as the polarization angles are varied. The superstrate was set to a refractive index of 1.0 (air) to suppress the liquid mode response $\lambda_T$ (following the trend that the smaller refractive index of the liquid compared to $LiNbO_3$ yields a much lower response) – the small dip at 520 nm was attributed to be the $\lambda_T$ (liquid) mode; this was so that we could primarily investigate the $\lambda_B$ mode only. Due to the symmetrical properties of the nanodiscs and their array periodicity, and the fact that the light was as close to normally incident as possible, we associate the variation of $\lambda_B$ solely to the birefringent properties of the $LiNbO_3$ crystal. As can be seen in Fig. 3, the wavelength $\lambda_B$ varies as a function of the polarization angle, where we find that it experimentally changes by up to 15 nm between 0° and 90°. We attribute the difference between simulated and experimental results to be from imperfections in the fabricated device.

This experiment shows that SPR structures on birefringent material can offer polarization sensitive optical transmission for potential applications. For instance, traditional plasmonic colour filters fabricated on glass substrates can only support a single wavelength for each designed pattern; a colour filter which adopts a highly birefringent substrate material may be able to support multiple transmission peaks that can be individually selected by adding a polarizer into the device. Following on from this, the wavelength shift at $\lambda_T$ caused by polarization change needs to be studied to give us a better understanding of the two resonance modes and the SPR sensing functionality on high refractive index materials.

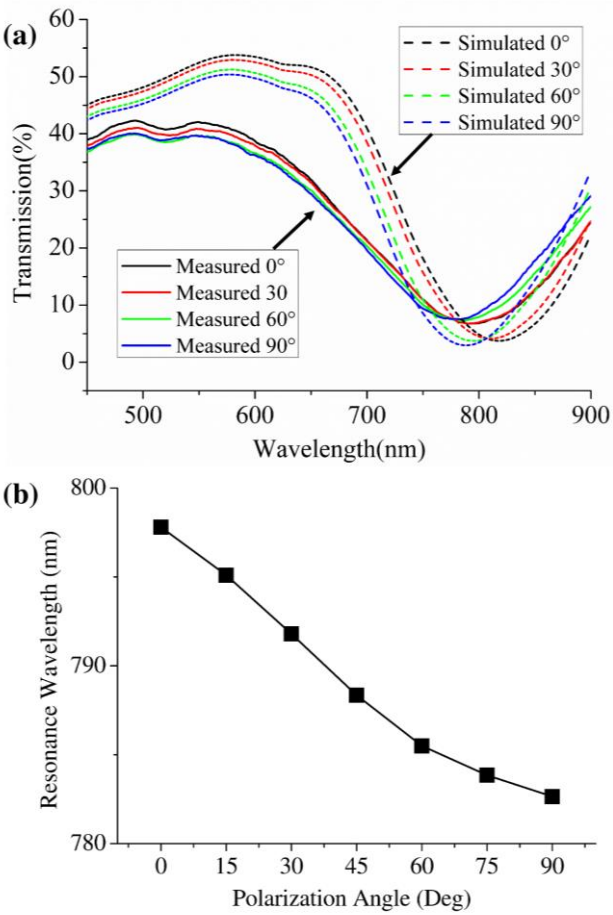


FIG.3. (a) Simulated and measured spectra of Au nanodisc arrays on $LiNbO_3$ surrounded by air. Data is recorded for four different polarization angles: 0° (x-polarized), 30°, 60°, and 90° (z-polarized). (b) Expanded experimentally measured resonance wavelengths of Au nanodisc arrays on $LiNbO_3$ for seven different polarization angles.

To examine the impact that birefringence makes to SPR sensing, experiments were carried out for different concentrations of glycerine-water solution on top of the sample surface in conjunction with polarization angle changes, and transmission spectra were simulated for polarization angle change (for water only). As seen in Fig. 4, since $\lambda_T$ is related to the SPR at the interface between the metal and water/glycerine solution it does not shift with polarization angle change (the vertical line markers between Figs 4(a) and 4(b) are present for ease of viewing). This is also apparent in the simulated results (Inset of Fig. 4(a)) where the $\lambda_T$ (top surface) SPR mode does not shift when the polarization is varied (even for unpolarized light). We should note that the transmission intensity differences for $\lambda_T$ between 0° and 90° (when comparing Figs 4(a) and 4(b)) are simply due to the refractive index mismatches between the birefringent substrate and liquid. Meanwhile, an

SPR at $\lambda_B$ is more sensitive to the refractive index change of the substrate, as expected, and so exhibits a shift in the spectrum after changing the polarization from x-polarized (0˚) to z-polarized (90˚). Experimental results show an average blue shift of the resonance wavelength at $\lambda_B$ by ~14nm for the two orthogonal polarizations, when using three different concentrations of water-glycerine solution (0% corresponds to purely water, 50% corresponds to 1:1 water-glycerine, and 100% is purely glycerine), which is comparable to the shift given in Fig. 3(b); the Inset of Fig. 4(b) shows a plot of the resonance minima at $\lambda_B$ for clarity.

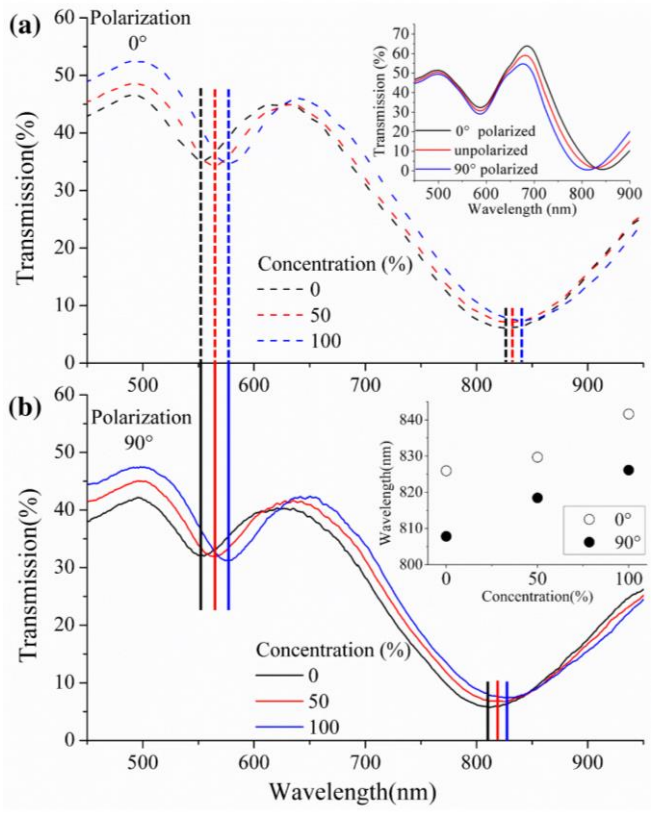


FIG.4. (a) Measured transmission spectra for different concentrations of glycerine-water solution using x-polarized light (0˚). Inset: Simulated results of the transmission spectra for water (*Black line*: x-polarized light. *Red line*: z-polarized light. *Blue line*: unpolarized light.) (b) Measured transmission spectra for different concentrations of glycerine-water solution using y-polarized light (90˚). Inset: Measured $\lambda_B$ minima of concentration-dependent wavelength shift, for 0˚ (*hollow* data) and 90˚ (*solid* data) polarizations**.**

Since the shift at $\lambda_B$ due to the polarization change is non-negligible, alignment of the light source and the sensor needs to be considered for a polarized light source. On the other hand, for a fixed polarization angle, the shift at $\lambda_T$ due to changes in liquid refractive index variation is larger than those for $\lambda_B$, and therefore the liquid mode has a higher sensitivity compared to the $LiNbO_3$ mode; as such, it is preferential to utilize $\lambda_T$ for sensing capabilities since it is also unaffected by substrate birefringence related effects.

In summary, we have fabricated Au nanodisc arrays on piezoelectric substrates using lift off process and our SPR sensor has the capability to be coupled with compatible SAW technology. We demonstrate that the Au nanodisc arrays exhibit refractive index dependent SPR properties which can be used for label free biosensing. We have also demonstrated polarization angle dependent transmission spectra, which arises from the birefringent $LiNbO_3$ substrate. It is concluded that for a substrate which has a refractive index differing by a large amount from the analyte, the SPR sensor should be designed targeting the liquid mode $\lambda_T$ as this provides a higher sensitivity than $\lambda_B$, and is not sensitive to the birefringence of the piezoelectric material. We believe that the integration between these Au nanodisc arrays and a SAW sensor can make the hybridized device an efficient, versatile platform for better studying the biomolecule binding process in real time.

The authors wish to thank all the technical staff of the James Watt Nanofabrication Centre at Glasgow University for their contributions. This work is supported by an EPSRC grant (The Multicorder, EP/K021966/1)

[1] B. Sepúlveda, P. C. Angelomé, L. M. Lechuga, and L. M. Liz-Marzán, Nano Today **4**, 244 (2009).

[2] S. Unser, I. Bruzas, J. He, and L. Sagle, Sensors **15**, 15684 (2015).

[3] J. N. Anker, W. P. Hall, O. Lyandres, N. C. Shah, J. Zhao, and R. P. Van Duyne, Nat. Mater. **7**, 442 (2008).

[4] K. A. Willets and R. P. Van Duyne, Annu. Rev. Phys. Chem. **58**, 267 (2007).

[5] M. Nirschl, F. Reuter, and J. Vörös, Biosensors **1**, 70 (2011).

[6] J. Vörös, Biophys. J. **87**, 553 (2004).

[7] K. Mitsakakis, A. Tsortos, and E. Gizeli, Analyst **139**, 3918 (2014).

[8] W. Tseng, J. Lin, W. Sung, S. Chen, and G. Lee, J. Micromechanics Microengineering **16**, 539 (2006).

[9] A. Renaudin, V. Chabot, E. Grondin, V. Aimez, and P. G. Charette, Lab Chip **10**, 111 (2010).

[10] F. Bender, P. Roach, A. Tsortos, G. Papadakis, M. I. Newton, G. McHale, and E. Gizeli, Meas. Sci. Technol. **20**, 124011 (2009).

[11] J. Homola, Anal. Bioanal. Chem. **377**, 528 (2003).

[12] S. S. Aćimović, M. A. Ortega, V. Sanz, J. Berthelot, J. L. Garcia-Cordero, J. Renger, S. J. Maerkl, M. P. Kreuzer, and R. Quidant, Nano Lett. **14**, 2636 (2014).

[13] A. Brolo, Nat. Photonics **6**, 709 (2012).

[14] S. Sanna and W. G. Schmidt, Phys. Rev. B - Condens. Matter Mater. Phys. **81**, 1 (2010).

[15] R. Weis and T. Gaylord, Appl. Phys. A Mater. Sci. Process. **37**, 191 (1985).

[16] See https://www.lumerical.com/ for more information; accessed 17 Mar 2016.

[17] P. B. Johnson and R. W. Christry, Phys. Rev. B **6**, 4370 (1972).

[18] S. W. Lee, K. S. Lee, J. Ahn, J. J. Lee, M. G. Kim, and Y. B. Shin, ACS Nano **5**, 897 (2011).

[19] K. Lodewijks, W. Van Roy, G. Borghs, L. Lagae, and P. Van Dorpe, 3001 (2012).

[20] L. F. Hoyt, Ind. Eng. Chem. **26**, 329 (1934).

[21] M. M. Miller and A. A. Lazarides, J. Phys. Chem. B **109**, 21556 (2005).